Water confined to a slab geometry: a review of recent computer simulation studies

2004 J. Phys.: Condens. Matter 16 S5371

(http://iopscience.iop.org/0953-8984/16/45/005)

INSTITUTE OF PHYSICS PUBLISHING JOURNAL OF PHYSICS: CONDENSED MATTER

J. Phys.: Condens. Matter **16** (2004) S5371–S5388 PII: S0953-8984(04)75664-7

Water confined to a slab geometry: a review of recent computer simulation studies

Ronen Zangi

The Groningen Biomolecular Sciences and Biotechnology Institute, Department of Biophysical Chemistry, University of Groningen, Nijenborgh 4, 9747 AG Groningen, The Netherlands

E-mail: r.zangi@chem.rug.nl

Received 20 January 2004
Published 29 October 2004
Online at stacks.iop.org/JPhysCM/16/S5371
doi:10.1088/0953-8984/16/45/005

Abstract

The dimensionality of a system largely determines the nature of any long range order that is possible in the solid phase. For this reason considerable effort has been directed towards elucidating the behaviour of materials under confinement and at interfaces. This has ranged from theoretical studies that predict that a truly two-dimensional solid cannot exist to studies on the use of confinement to promote solidification in thin films. In this paper we review the results of recent molecular dynamics simulations of water confined to a slab geometry. The simulations predict that the freezing and melting of a monolayer and a bilayer of liquid water can be induced at ambient conditions by changing the distance between two confining parallel walls. The confined ice phases are stable only for a small range of plate separations. This can be explained by the ability of the structure of the confined ice phases to achieve optimal distance and angle of hydrogen bonds only for a small range of gap values. Above the film thickness of a bilayer, the degree to which the solid phase is enhanced due to confinement is insufficient to freeze liquid water at ambient conditions. It is also found that a bilayer of liquid water can supports two different phases of liquid water that differ in the local ordering at the level of the second shell of nearest neighbours and in the density profile normal to the plane. These high- and low-density phases of confined liquid water suggest the intriguing possibility of a liquid–liquid transition as a function of the film thickness.

(Some figures in this article are in colour only in the electronic version)

1. Introduction

No chemical compound has been studied more extensively than water. Water plays a critical role in living systems and most terrestrial chemical reactions, and as such is arguably the

most important solvent in nature. Water is also fascinating from the physical perspective due to its many unique properties compared to other liquids, the most famous of these being the density maximum at 4 °C. The underlying reason for such anomalous behaviour is the unique capability of water to form extensive hydrogen bonding interactions. Knowledge of the behaviour of water confined to different geometries, with length scales comparable to that of its diameter, is crucial for understanding many biological and geological processes as well as for advancing technological developments at the nanoscale.

When liquids are confined between solid walls separated by only a few molecular diameters, their structural and dynamical properties are drastically altered compared to that of the bulk. This can be attributed in part to the changes that occur in liquids in the vicinity of a rigid wall and in part to the two-dimensional character of the system. It is well known that liquid next to a wall undergoes stratification that extends 2–3 molecular diameters into the bulk [1]. The density profile along the direction perpendicular to the wall (the transverse density profile) is qualitatively similar to the radial distribution function of a uniform liquid. Although the former is a one-body distribution function, it can be viewed as the pair correlation function (two-body distribution function) of all the particles with another particle that is fixed in space with an infinite diameter (i.e. zero curvature) which is identified as the wall. The magnitude and the range of the layered structure formed depend on the density of the liquid and on the interactions of the particles with the wall. However, wall induced layering occurs also in hard sphere systems. It originates from an excluded volume effect and yields the most efficient packing geometry. If the density of the liquid is low enough the transverse profile has only a single peak and resembles the radial distribution function of a uniform gas.

As a consequence of the layered structure, the normal stress acting on the walls (known as 'solvation forces') as a function of the distance between the walls, H, oscillates between attraction and repulsion with a periodicity approximately equal to the molecular diameter [2–6]. These experimentally observed oscillations have also been seen in theoretical treatments of model films using integral equations [7–9], density functionals [10, 11] and computer simulations [12–18] and emerge from an abrupt addition/removal of whole layers as H is increased/decreased. In order to observe the oscillatory nature of the solvation forces, the confining walls have to be smooth on the molecular scale. If the gap between the confining walls is larger than 7–8 particle diameters, then the dynamical properties of the liquid are similar to those of the bulk. In this case, the layering against each of the walls can be regarded independently and the liquid retains its fluidity. At wall separations smaller than about seven particle diameters stratification is enhanced. Then, the effective viscosity and molecular relaxation times of several liquids increase by several orders of magnitude and the film develops a yield stress, indicating a transition to a solid-like state [2, 5, 18–23]. In some cases the changes in the film properties were attributed to a glass transition [24]. Molecular dynamics (MD) simulations also provide evidence for transitions to both solid [16, 25–29] and glassy states [26, 30] as H is decreased.

Why is solidification promoted under confinement? The confined liquid state has a reduced entropy, compared to that of the bulk, due to the restriction in the motion along the transverse direction. Therefore, the difference between the free energy of the liquid phase and that of the solid phase is smaller for the confined system than it is for the bulk. In some cases, the more stable state at ambient conditions for a system under confinement corresponds to the crystalline phase. It is found that the degree of the solid phase enhancement depends on the nature of the liquid studied. For confinement induced freezing to take place it is necessary that the molecules are able to establish in-plane interparticle connectivity. If the interactions between the particles in the slab configuration are hindered it is possible that the free energy of the solid state is also lowered and that the freezing point may shift to lower temperature

than for the bulk. Therefore, the question is whether water under confinement can generate an effective two-dimensional network of hydrogen bonds so that its freezing temperature is higher than that of the bulk.

Another unique property of water is its rich polymorphism of crystalline phases. No other known substance exhibits such a variety of forms. This is traceable to the anomalous density increase on melting of ordinary ice. In spite of the diversity of the crystallographic cells and the symmetries, the structures of the various ice forms have a simple common pattern that is known as the 'ice rules' [31]. The structures of the ice phases are all built of discrete water molecules which are little altered from their molecular configuration in the vapour phase. Each water molecule forms four asymmetric hydrogen bonds (donating protons to two other water molecules and accepting protons from another two) making a tetrahedral bond framework that extends across the entire crystal [32–34]. While in hexagonal and cubic ice the tetrahedral geometry is nearly perfect, in most other ice phases distortions from ideal geometry occur. This involves substantial bending of the hydrogen bonds at the expense of bond strength. The extent of the hydrogen bond bending increases progressively with the packing density (except for ices VII and VIII). Nevertheless, there is no change in the molecular geometry of the individual water molecule. Hydrogen bonding interactions are insufficient to initiate the rehybridization of the sp^3 hybridized oxygen atom and thus a change in either the molecular H–O–H angle or in the spatial distribution of the electron lone pairs. Although, the hydrogen bonding network formed by water is incompatible with a two-dimensional geometry it is expected that the molecular geometry of the individual water molecule is preserved and the degree of the hydrogen bond distortion (from a collinear angle) would be in the range of the distortions found in the high-pressure bulk ice phases.

2. Water monolayer

The results described below were obtained by MD simulation of water confined to a monolayer. The five-site, tetrahedrally coordinated, TIP5P model [35] was used to describe the water molecules. The TIP5P water model was chosen because it represents the electron lone pair sites explicitly. This favours formation of hydrogen bonds in a tetrahedral geometry. The water molecules were confined between two parallel walls that are separated by a distance H. Each wall was modelled by a triangular arrangement of atoms out of registry with respect to the other wall. The wall–water interactions were modelled by a Lennard-Jones potential representing approximately the van der Waals interaction between a water molecule and a quartz (SiO_2) surface. Thereby, the simulations pertain only to surfaces that cannot form hydrogen bonds with the water molecules. All simulations were performed using a constant number of particles, N, and each system was coupled to a thermal bath using a Berendsen thermostat [36]. Additional details about the methodology used can be found elsewhere [37].

Results from simulations with 780 water molecules, for lateral pressures, P_l, of 1 and 100 bar and temperature $T = 300$ K, are presented below. The lateral diffusion coefficient for plate separations in the range $0.41\ \text{nm} \leqslant H \leqslant 0.59\ \text{nm}$ is shown in figure 1. At $H = 0.51$ nm there is a sharp drop of 3–4 orders of magnitude in the value of the lateral diffusion coefficient indicating that the water molecules of the monolayer transform to a frozen state. At $H = 0.57$ nm the lateral diffusion coefficient increases again to values that characterize high fluidity. At this point the monolayer transforms into a bilayer of liquid water. The value of the lateral diffusion coefficient of liquid water in the monolayer is higher than in the bilayer due to the presence of interlayer hydrogen bonds in the bilayer resulting in an increase in connectivity and a decrease in mobility. It is also slightly higher than the diffusion coefficient of the experimental value of the bulk ($2.30 \times 10^{-5}\ \text{cm}^2\ \text{s}^{-1}$) and the TIP5P model value [38] ($2.62 \times 10^{-5}\ \text{cm}^2\ \text{s}^{-1}$) at $T = 298$ K. The degrees of spatial order of the oxygen atoms as

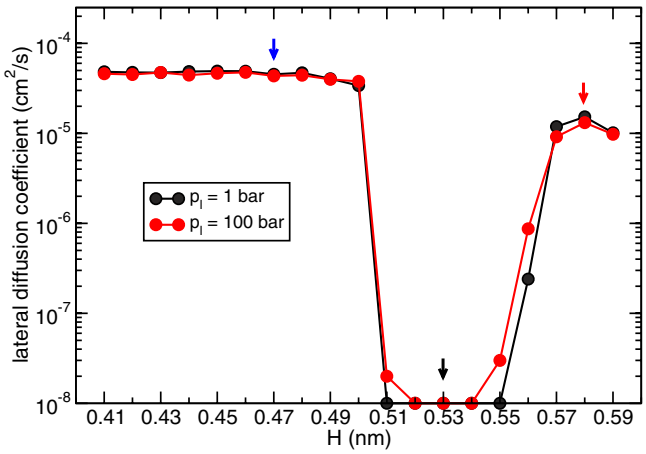

Figure 1. The lateral (in-plane) diffusion coefficients for a monolayer (0.41 nm $\leqslant H \leqslant$ 0.56 nm) and a bilayer ($H \leqslant 0.57$) of water ($N = 780$ molecules) as a function of the distance between the confining parallel plates at $T = 300$ K. This figure was taken from [37].

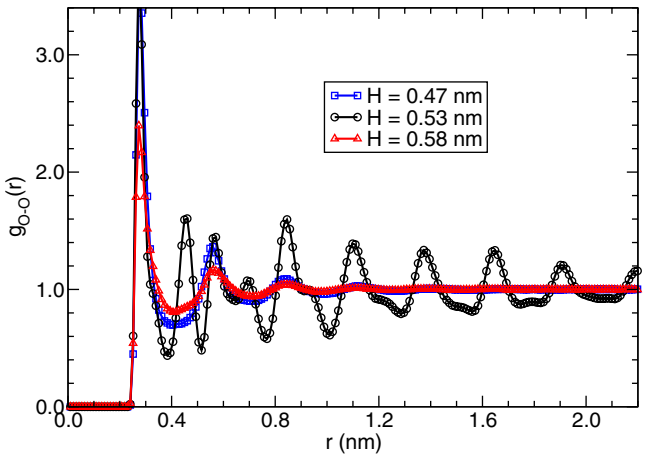

Figure 2. The oxygen–oxygen radial distribution function for a monolayer of liquid water ($H = 0.47$ nm), monolayer ice ($H = 0.53$ nm) and a bilayer of liquid water ($H = 0.58$ nm).

indicated by the O–O radial distribution functions for $H = 0.47$, 0.53 and 0.58 nm are shown in figure 2. The short range order in the plots corresponding to $H = 0.47$ and 0.58 nm reflects the disorder of the liquid phase. However, the long range order at $H = 0.53$ nm indicates that the system has the characteristics of an ordered crystalline phase. In the calculations of the radial distribution function, the normalizing volume element was taken be cylindrical in accordance with the system geometry.

This freezing transition occurs at a temperature ($T = 300$ K) well above the freezing temperature of a bulk TIP5P water ($T < 270$ K). The first peak in the radial distribution function in all phases appears at the same value of the interparticle distance ($r = 0.28$ nm). For the monolayer ice the second peak is located at ($r = 0.45$ nm), similar to the location that appears for bulk water. However, for the two liquid phases of water ($H = 0.47$ and 0.58) the second-nearest neighbour peak around 0.45 nm is missing. This is a consequence of arranging particles in a single plane where the next nearest neighbours of a three-dimensional arrangement

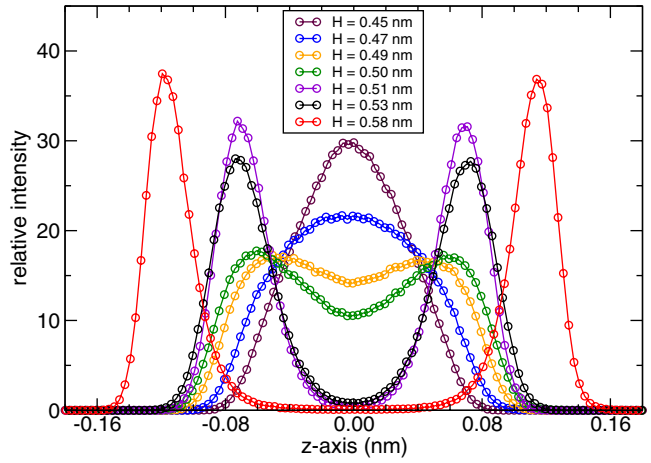

Figure 3. The transverse distribution of the density of oxygen atoms for different plate separations, H. This figure was taken from [37].

are not present. This implies that the monolayer ice is characterized by a correlated out-of-plane configuration while the two layers of liquid water at $H = 0.58$ nm (which is the smallest gap between the walls that support a bilayer system) is uncorrelated and can be regarded as two monolayers. This argument can be shown in the transverse density profile displayed in figure 3. The distributions reveal that the liquid state of the monolayer is characterized by a unimodal distribution. As H approaches the transition point ($H = 0.51$ nm), the distribution starts to develop two peaks adjacent to the walls. There is a clear bimodal character for $H \geqslant 0.51$ nm. A transformation from a homogeneous to a split normal density distribution of each layer in confined solids as a function of the parallel plate separation is a fingerprint of a buckling transition. Buckled phases were first observed in monolayers [39–44] and later in multilayers [45, 46] of colloidal particles. The transition to a bimodal distribution of the transverse density is coupled to an in-plane order–disorder transition. The lateral ordering takes the form of linear or zigzag rows of particles which are buckled against each other. The manifestation of the buckling transition enhances as the number of layers decreases.

Figure 5 shows a configuration after equilibration from a simulation of monolayer water ($H = 0.47$ nm), monolayer ice ($H = 0.53$ nm) and bilayer water ($H = 0.58$ nm). The structures reflect the picture that emerges from the behaviour of the dynamics, the normal density profiles and the radial distribution functions. The ice monolayer has an in-plane rhombic symmetry with respect to the positions of the oxygen atoms. The out-of-plane positions correspond to a linear buckled phase. Figure 4 displays the distribution of the hydrogen bond angles. It shows that this out-of-plane displacement, together with the rhombic arrangement of the nearest neighbours, results in a hydrogen bond angle distribution with maxima at 164° and 139°. At the same time it allows each water molecule to be involved in four hydrogen bonds according to the Bernal–Fowler ice rules [31]. Each water molecule donates to and accepts from its nearest neighbours present in the other vertical plane one hydrogen bond (this corresponds to the lower degree of the hydrogen bond bending, the peak at 164°). In addition each water molecule donates to and accepts from its nearest neighbours present in the same vertical plane one hydrogen bond (this corresponds to the higher degree of the hydrogen bond bending, the peak at 139°). The situation where half of the water molecules donate (and the other half accept) two hydrogen bonds from their nearest neighbours in the same plane is unfavourable since the molecular H–O–H angle is smaller by ∼6° than the two

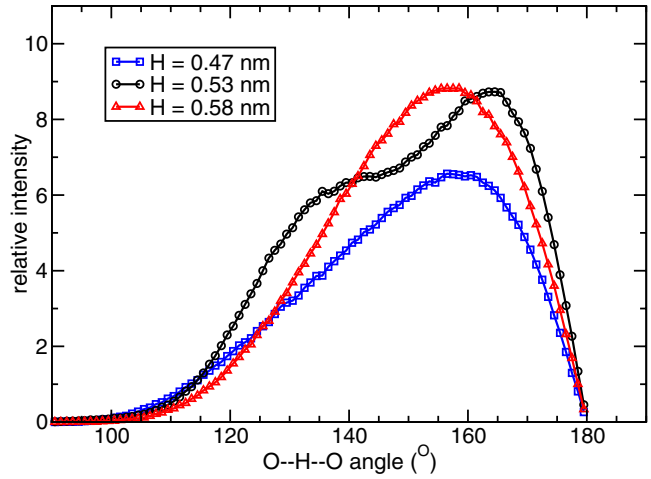

Figure 4. The hydrogen bond angle distribution. The ratio of the areas under each of the plots corresponds to the ratios of the average numbers of hydrogen bonds per molecule, namely, 2.8:3.8:3.5 for $H = 0.47$, 0.53, 0.58 nm respectively.

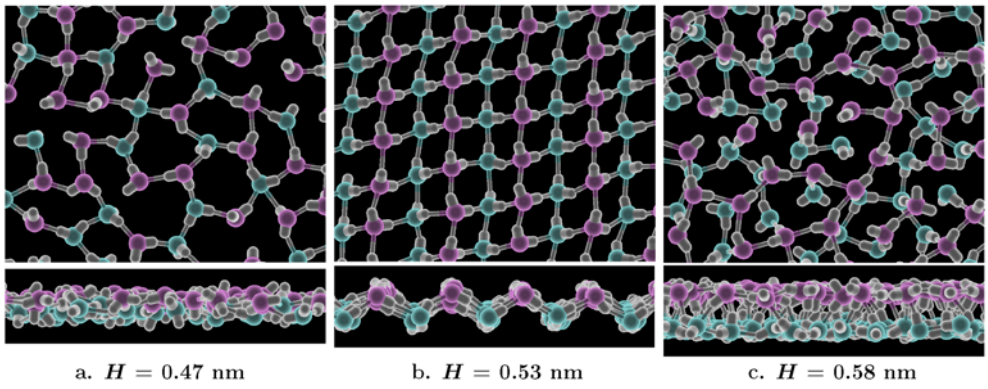

Figure 5. (Colour online) Lateral (in-plane) and transverse (out-of-plane) views of instantaneous configurations for (a) a water monolayer, (b) an ice monolayer and (c) a high-density bilayer of liquid water. Hydrogens are depicted in white. Oxygen atoms that lie above and below the mid-plane along the normal axis are depicted in dark grey (magenta) and light grey (cyan), respectively. This figure was taken from [37].

molecular angles that involve the lone pair electrons. This situation would lead to a greater distortion of the hydrogen bonds. In the liquid phase the hydrogen bond angle distribution is unimodal with a maximum at 159° for the monolayer and at 157° for the bilayer. The density of the ice monolayer is in the range 0.90–0.91 g ml^{-1}. This is higher than the density of the water monolayer (0.79–0.87 g ml^{-1}) but lower than the density of the bilayer water examined in this study (1.11–1.16 g ml^{-1}).

In contrast to the structure of the hexagonal ice that is characterized by a random arrangement of the hydrogen atoms, in the ice monolayer the positions of the hydrogen atoms are ordered. This can be explained by calculating the residual entropy (the entropy at low temperatures) of the ice monolayer. As shown by Pauling [47] for the hexagonal ice, I_h, the calculations reduce to the evaluation of the total number of possible orientations of the water molecules, W. The treatment considers the oxygen atoms fixed in space. In rhombic

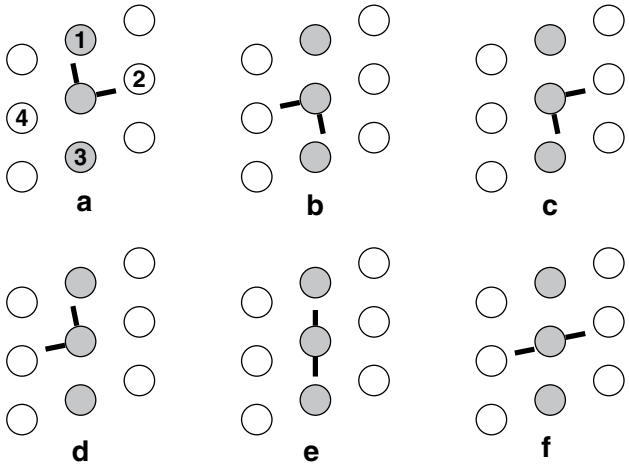

Figure 6. A schematic diagram displaying the possible hydrogen bond connectivity of a water molecule with its nearest neighbour in an ice monolayer. Only the hydrogen atoms of the central molecule are shown. Different shading depicts oxygen atoms in different planes. Note that the configuration with the lowest degree of hydrogen bond distortion (i.e. the configuration with the lowest energy) is only doubly degenerate (corresponding to configurations (a) and (b)).

symmetry, each water molecule is surrounded by four nearest neighbours. Figure 6 shows the oxygen atoms of the water molecules in a buckled rhombic symmetry (different colours depict atoms in different planes). Only the hydrogen atoms of the central molecule are shown. The configuration shown in (a) is the one that we found in the monolayer ice and it has the lowest degree of hydrogen bond distortion; thus, it corresponds to the configuration with the lowest energy. It is equivalent to the configuration shown in (b), and can be obtained by rotating the central water molecule in (a) by 180°. The configurations in (c) and (d) are not equivalent to (a) since the O_2–O–O_3 and O_4–O–O_1 angles are larger than the O_1–O–O_2 angle which led to a larger distortion of the hydrogen bonds. It is also possible to fill the entire space by alternating the configurations shown in (e) and (f). However, the configuration in (e) is unfavourable in comparison to that in (a) since the molecular H–O–H angle is smaller by $\sim 6°$ than the two molecular angles that involve the lone pair electrons, a situation which also leads to a greater distortion of the hydrogen bonds. Therefore, the number of possible orientations for the hydrogen bond connectivity of a water molecule with the nearest neighbour molecules (labelled 1, 2, 3 and 4) that have the lowest energy is 2. The chance that the neighbouring molecules will permit a given orientation is $1/4$. In (a) for example, there is a probability of $1/2$ that molecule 1 will point the lone pair electrons towards the central molecule, and a probability of $1/2$ that molecule 2 will do the same. The probability that molecule 3 and 4 will point their hydrogens towards the central molecule will be taken into account when summing over all N molecules. The total number of configurations for N molecules is then $W = (2/4)^N$, which mean that there is no residual entropy, $S_0 = k_B \ln(W)$, in the ice monolayer. Therefore, the hydrogen positions must be ordered, as is evident in figure 5(b). In hexagonal ice, I_h, all six orientations are possible (they are equivalent due to the crystal symmetry) and the residual entropy is $Nk_B \ln(6/4)$.

The freezing transition to a monolayer ice was also obtained in simulations performed at constant area, A, and plate separation, H (N, T, A, H ensemble). This and the strong van der Waals loop observed for the lateral pressure–area isotherm indicate that the transition is first order [37]. In a set of simulations, the freezing is induced by changing the area A. Figure 7 shows that for a certain value of A there is a phase seperation between water

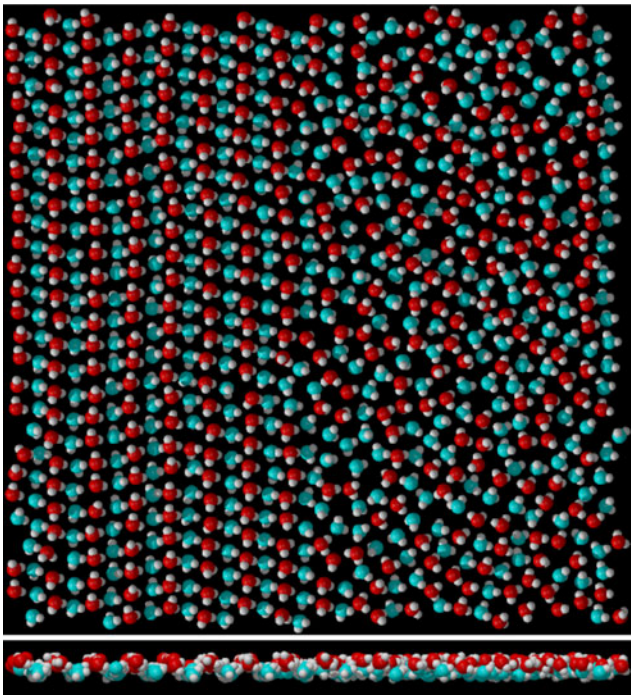

Figure 7. Results from a simulation at constant number of particles, N, area, A, plate separation, $H = 0.50$ nm, and temperature, $T = 300$ K, showing the coexistence between a water monolayer and an ice monolayer obtained at $A = 57.0$ nm^2. This figure was taken from [37].

monolayer and ice monolayer. In addition, the potential energy of the system displays a sharp linear decrease which is a consequence of the lever rule partitioning of a first-order transition. Other simulations in which the system is coupled to a thermal bath in the range 265 K $\leqslant T \leqslant$ 380 K indicate that at appropriate values of H freezing can also be induced by decreasing the temperature. They also indicate that the region of stability (in terms of H and A) of the ice monolayer increases as the temperature decreases. However, at small wall separations ($H \leqslant 0.45$ nm) and low lateral pressures ($P_l \leqslant 3$ kbar) the system remained liquid even at temperatures as low as 265 K.

As mentioned before, the simulations pertain only to surfaces that will not disrupt the hydrogen bond connectivity of the water molecules. The structure of water next to substrate can be changed due to competing interfacial interactions [48]. They can induce epitaxial freezing with the underlying lattice structure of the surface. The structure of water were reported on the surfaces of muscovite mica [49–53], Ru(001) [54, 55], MgO(100) [56], NaCl(100) [57] and confined in an organic slit-shaped nanospace [58].

When interfacial interactions dominate the system, information concerning the intrinsic physics of confinement is hidden. Porter and Zinn-Warner studied water confined between mercury surfaces, a system where the wall–water interaction is relatively weak [59, 60]. They found that the Young's modulus of two-dimensional ice shows a maximum value (of ∼20% of that of bulk ice I_h) around a junction separation of 0.58 nm. The elastic modulus changed non-monotonically by a few orders of magnitude with small changes in film thickness. This behaviour led the authors to raise the intriguing possibility of a confinement-driven buckling transition occurring as a function of film thickness in the system. Although these experimental studies were conducted at $T = 265$ K, we argue that the origin of this behaviour of water

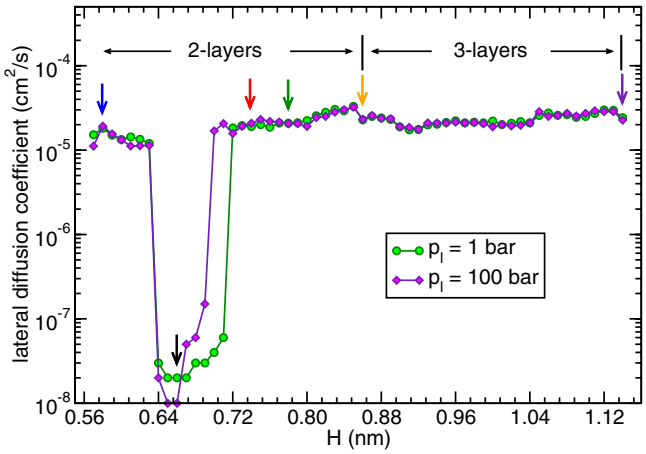

Figure 8. The lateral (in-plane) diffusion coefficients of water ($N = 1200$) as a function of the distance between the confining parallel plates for two values of the lateral pressure, P_l, at $T = 300$ K. This figure was taken from [61].

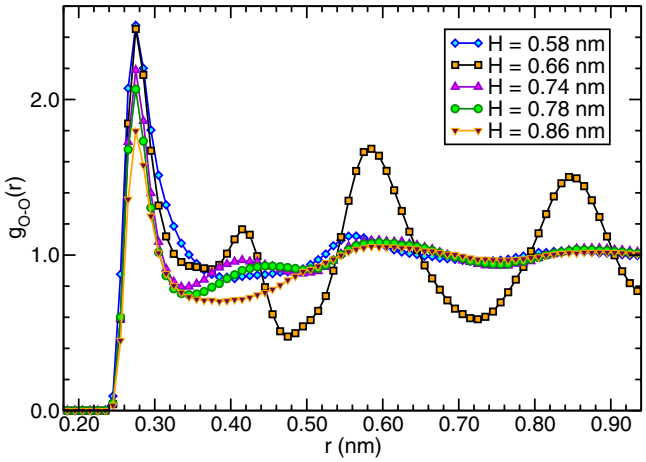

Figure 9. The radial distribution function of oxygen atoms. Note that the location of the second peak in the bilayer ice ($H = 0.66$ nm) is shifted to smaller values of r compared to the hexagonal ice case while in the liquid phases at $H = 0.58$ and 0.86 nm it is completely missing.

is confinement induced freezing (to buckled ice monolayer) and melting as predicted by the simulations.

3. Bilayers and trilayers of water

The structure of the bilayer of liquid water shown in figure 5(c) is strained, as its radial distribution function is missing the peak at $r = 0.45$ nm. The restricted distance between the confining walls acts as a constraint and prevents the system from relaxing to a more optimal configuration. The existence of a constrained liquid structure suggests a transition to a more relaxed state upon increasing H.

Results from simulations with 1200 water molecules, for lateral pressures, P_l, of 1 and 100 bar and a temperature of $T = 300$ K, are presented below. Figure 8 shows the lateral diffusion coefficient for plate separations in the range 0.57 nm $\leqslant H \leqslant$ 1.14 nm. A similar

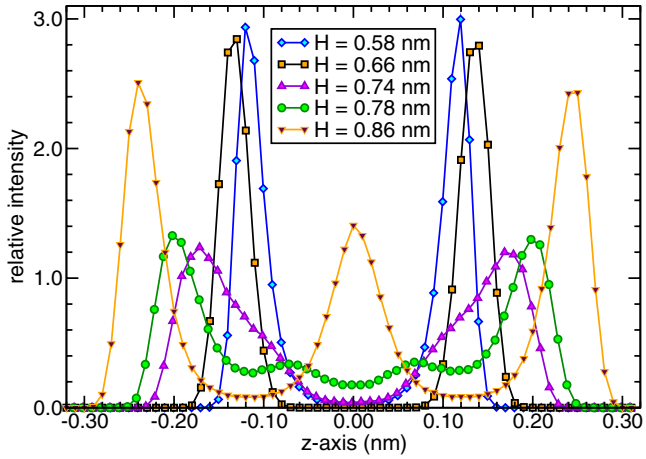

Figure 10. The transverse density profile of oxygen atoms for different values of plate separation H.

behaviour that characterizes the monolayer system is observed in this case as well. At $H = 0.64$ nm the lateral diffusion coefficient drops by about three orders of magnitude. At this point, the dynamics of the molecules changes from free diffusion to small amplitude fluctuations around fixed positions with occasional cooperative jumps. Figure 9 displays the oxygen–oxygen radial distribution functions for various plate separations. The short range order in the plots corresponding to $H = 0.58$, 0.74, 0.78 and 0.86 nm reflects the disorder of the liquid phase. However, the long range order at $H = 0.66$ nm (the peaks in $g(r)$ persist throughout the entire box [61]) indicates that the system has adopted a crystalline phase. Examination of the density profile along the transverse direction (figure 10) of the oxygen atoms of the bilayer ice (for the entire range of values of H that span its region of stability) reveals that the distribution is bimodal: one peak for each layer. Despite the absence of a buckling transition as occurred for the ice monolayer, the degree of the hydrogen bond distortions is relatively small. The O–H–O angle distribution is peaked at around 155° [61]. The average number of hydrogen bonds per molecule in the bilayer ice is 3.8 while in the bilayer phases of liquid water it is 3.4. Figure 11 shows the instantaneous configurations for $H = 0.66$, 0.74 and 0.86 nm. The in-plane symmetry of the oxygen atoms in the ice bilayer is rhombic with a distorted in-registry arrangement between the two layers. The hydrogen positions are ordered. The out-of-plane hydrogen bond connectivity exhibits order that is built of two alternating rows of water molecules that point their hydrogens toward the oxygens present in the other layer. The density of the bilayer ice is estimated to be in the range 1.01–1.05 g ml^{-1}. The freezing and melting transitions were found to be first order; however, the lateral pressure–area isotherms indicate that the discontinuity is much weaker than that observed for the water monolayer [61].

On further increase of the distance between the two confining walls, the bilayer ice melts to a bilayer of liquid water that is different to the one found at 0.57 nm $\leqslant H \leqslant$ 0.63 nm. The effect of higher lateral pressure is to destabilize the ice bilayer as shown in figure 8. The melting transitions occur at $H = 0.72$ nm for $P_l = 1$ bar and at $H = 0.70$ nm for $P_l = 100$ bar. The transverse density profiles of the oxygen atoms of the large-H and small-H bilayers of liquid water are different. The curve for the liquid phase that is stable at larger values of the plate separation indicates that the distribution of each of the two layers is split. This is shown in figure 10 for $H = 0.74$ and 0.78 nm (for $H = 0.74$ nm the splitting is evident only as 'shoulders' on the main peaks). The ratio between the intensity of the peaks is very similar to

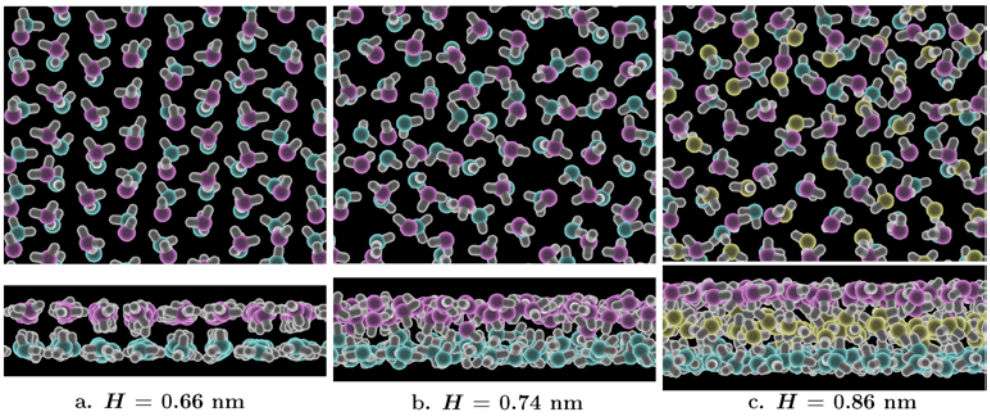

Figure 11. (Colour online) Lateral and transverse views of instantaneous configurations for (a) a bilayer ice, (b) a low-density bilayer of liquid water and (c) a trilayer of liquid water. Oxygen atoms in different layers are depicted in different grey scale (colours).

those of confined solids corresponding to a two-layered buckled phase [45, 46]. However, in the liquid phase there is an overlap between the peaks resulting from diffusion of particles between the different planes. The density of the small-H bilayer of liquid water is estimated to be in the range 1.02 g ml^{-1} $\leqslant H \leqslant$ 1.11 g ml^{-1} (high-density phase) while that of the large-H bilayer of liquid water is in the range 0.87 g ml^{-1} $\leqslant H \leqslant$ 0.97 g ml^{-1} (low-density phase). In addition to the different behaviour of the transverse density profiles, the radial distribution functions of the oxygen atoms of the high- and low-density liquid phases confined to a bilayer also exhibit a qualitative difference. The second peak in the radial distribution function for the bilayer ice is shifted toward a lower value of the interparticle separation ($r = 0.41$ nm) as compared to that in bulk hexagonal ice. This indicates distortions from ideal tetrahedral coordination around each water molecule, which has also been observed experimentally for bulk ice phase [32–34] and bulk liquid water [62] at higher pressures. In this case, the accommodation of neighbours at distances in the range 0.3–0.4 nm (which allows structures with high densities) is too far for direct hydrogen bonding with the central molecule, but still close enough for dispersion interactions to be significant. The second peak of the radial distribution function of the low-density bilayer of liquid water is also at $r = 0.41$ nm for $H = 0.74$ nm. However, it shifts to larger values of around $r = 0.45$ nm (i.e. to a more optimal configuration) as the gap between the confining walls increases ($H = 0.78$ nm). Hence, the low-density liquid phase has a local ordering similar to that of the bilayer ice, whereas the high-density liquid phase has a local ordering similar to that of a monolayer of liquid water. The shift of the second peak in the radial distribution function to lower values of r was also observed in x-ray and neutron scattering experiments on liquid water confined in pores of poly(2-hydroxyethylmethacrylate) [63], in Vycor glass [64, 65] and at a hydrophobic surface [66]. These studies concluded that the molecular structure of water in an environment that disrupts its ability to establish a tetrahedral network of nearest neighbours exhibits a distortion at the second-neighbour level. In these cases, a hump in the radial distribution function at around $r = 0.37$ nm is observed while the packing of the first neighbours is not significantly affected.

These results suggest that at higher temperatures or at higher lateral pressures, where the ice bilayer becomes unstable with respect to either of the liquid phases, a direct transition between the two liquid phases would be possible. Computer simulations of supercooled bulk liquid water suggest the existence of a second critical point below which the liquid phase separates into high- and low-density liquid phases [67–69]. It has been suggested that these two liquid phases

of water are closely related to the phases that exist at lower temperatures, namely, low-density amorphous ice ($\rho = 0.94$ g ml^{-1}) and high-density amorphous ice ($\rho = 1.19$ g ml^{-1}) [70]. A first-order transition between these two amorphous phases of ice is induced by increasing the pressure. Structural analysis by means of x-ray diffraction showed that while the first peak in the radial distribution function is hardly changed, the second peak in the high-density amorphous ice is broad and split into two peaks near 0.37 and 0.47 nm [71]. Experimental evidence for such a liquid–liquid transition in water is hard to obtain due to nucleation that occurs in that region of the phase diagram; however, a liquid–liquid transition has been experimentally observed in fluid phosphorus [72]. A liquid–liquid phase transition has been reported also in Monte Carlo studies of confined water between a bilayer liquid with a split normal density profile and a trilayer liquid at $T = 235$ K with the ST2 model potential for water [73]. Another study using a restricted ensemble Monte Carlo method predicted the existence of four supercooled bulk liquid water phases at $T = 235$ K [74, 74]. We note that it is argued that a liquid–liquid phase transition in a single-component system is also possible even if there is only one crystal structure and no density anomaly [75].

A transition to a trilayer of liquid water occurs at $H = 0.86$. At this value of H, the liquid phase has the same structure as the monolayer and the high-density bilayer of liquid water. The radial distribution function (figure 9) shows that the second peak (located at $r = 0.41$ nm for the low-density bilayer of liquid water) is missing. It is found that the same structural properties are present when the system transforms to a four-layer liquid system ($H = 1.14$ nm) [61]. This is due to the fact that when the value of H is just enough to allow a transformation to a larger number of layers, the arrangement of the water molecules with respect to each other has to be modified due to the spatial constraints and the resulting liquid phase has a higher density. No freezing was observed at any value of plate separation that confined water to three layers at $T = 300$ K and ambient pressures (figure 8). Further simulations of water at the same conditions confined to 4–8 layers (1.15 nm $\leqslant H \leqslant 2.56$ nm) also indicate that water remains in the liquid phase (the lateral diffusion coefficient was found to be in the range $(2\text{–}3) \times 10^{-5}$ cm^2 s^{-1}) which is comparable to the diffusion coefficient of the bulk. This means that above the film thickness of a bilayer, the degree to which the solid phase is stabilized due to confinement is insufficient to freeze liquid water at ambient conditions. These findings are consistent with experimental measurements of the effective viscosity of water confined between mica surfaces [76] and can be attributed to the incompatibility between the tetrahedral arrangement of water and a slab geometry.

4. The influence of an electric field

When a sample of a polar liquid is exposed to an external electric field it undergoes polarization. At small electric fields the polarization is linearly proportional to the applied field. At high electric fields, deviations from linearity occur and the polarization eventually saturates. This behaviour for the case of bulk liquid water has been observed experimentally [77] and computationally [78–82]. It is found that the polarization curve fits well to the classical Langevin function. Thus, at high field strengths the polarization becomes constant and the resulting dielectric constant falls to unity. The favourable energetic interaction of the electric field with the dipole moment of the molecules reduces the entropy of the liquid phase due to the restriction of the orientational degrees of freedom along axes perpendicular to the applied field. Therefore, the difference in entropic contribution to the free energy between the liquid phase and the solid phase diminishes. In this case, if the entropy reduction is large enough and the interactions between the molecules are strong, the most stable phase would correspond to the crystalline phase. This phenomenon was demonstrated by studies of substrate nucleation of water by polar and non-polar amino acid crystals [83]. It was found that the crystals that

have a polar axis induce freezing at temperatures 3–5 °C higher than the crystals that do not have a polar axis. Since the substrate crystal structures did not have any match with the crystal structure of ice, the findings were interpreted in terms of an electric field mechanism that helped align the water molecules into a proton ordered ice nucleus, polar along its hexagonal axis. This mechanism for explaining the change in the freezing temperature is essentially kinetic in origin. A thermophysical explanation for the observed behaviour which predicts an elevation of the equilibrium freezing temperature was also offered [84]. The significance of the results is that an electric field mechanism may be of general applicability for ice nucleation.

In computer simulations, upon decreasing the temperature, phase trajectories tend to become trapped in regions corresponding to metastable glassy states [67]. Within the timescale of a typical simulation, such glassy states prevent the spontaneous homogeneous nucleation of ice. However, due to the promotion of freezing under the action of an electric field, several computational studies have reported spontaneous freezing of bulk liquid water [85–90]. It is found that under a field strength of about 5 V nm^{-1} and at temperatures of $T \sim 250$ K bulk liquid water undergoes crystallization to cubic ice. At lower temperatures (225–240 K) and at pressures of 3–5 kbar the water crystallizes to a previously unknown polymorph of ice which was denoted ice XII. Freezing to a crystalline phase was also observed in simulations of water between two charged platinum surfaces, 4 nm apart. It was found that when the charge density of the surface is high enough (35.40 μC cm^{-2} corresponding to an external electric field of 40 V nm^{-1}), water at a temperature of $T = 300$ K restructures itself and eventually crystallizes into a structure with domains of distorted cubic ice [91]. Depending on its strength, an electric field can weaken or destroy the hydrogen bonding network [92]. The anomalous behaviour of the polarization with increasing temperature observed in medium-sized water clusters has been attributed to an interplay between the water–water interactions and the interaction of the electric field with the water molecules [93, 94].

The following results were obtained from constant volume simulations with 1200 water molecules at $T = 280$ K, $H = 0.92$ nm with an applied, static and uniform, electric field (with magnitude of 5 V nm^{-1}) along the y-axis. The strong electric field applied in computational studies is necessary to accelerate the process of homogeneous nucleation which in many cases would otherwise far exceed typical simulation times. Field strengths of $\sim$5 V nm^{-1} are comparable to that experienced by water molecules within molecular distances from the surfaces of certain types of biopolymer [95]. It is also comparable to the fields generated by cracks in crystals [83] and within the operating range of lasers. Crystallization of confined liquid water under the influence of an external electric field along the lateral direction was observed during the simulations at certain plate separations [96]. A plate separation of $H = 0.92$ nm corresponds to a slab with the thickness of three layers of water. The structure of ice obtained at low densities $A = 46.24$ nm^2 ($\rho = 0.85$ g ml^{-1}) corresponds to the cubic ice phase. The in-plane structure of the hydrogen bonding network forms hexagonal rings. However, the rings are elongated along the y-axis, the direction of the applied electric field. The oxygen atoms that form the rings do not lie in the same plane. Upon lateral compression to $A = 36.00$ nm^2 ($\rho = 1.09$ g ml^{-1}), a first-order transition to a high-density ice phase takes place. The in-plane symmetry of all three layers is rhombic, the same as that of the in-plane structure of the monolayer and the bilayer ice phases found in the absence of an electric field. The structure of the two ice phases found can be seen in figure 12 for $A = 40.96$ nm^2. It corresponds to a coexistence between the low-density and high-density ice phases with approximately equal amounts of each phase. For both ice phases the positions of the protons are ordered in such a way that the dipole moment of the water molecule is aligned along the applied field. The pair correlation function of the oxygen atoms for the two phases in isolation and for the system in coexistence is displayed in figure 13. The curve for $A = 36.00$ nm^2 exhibits a

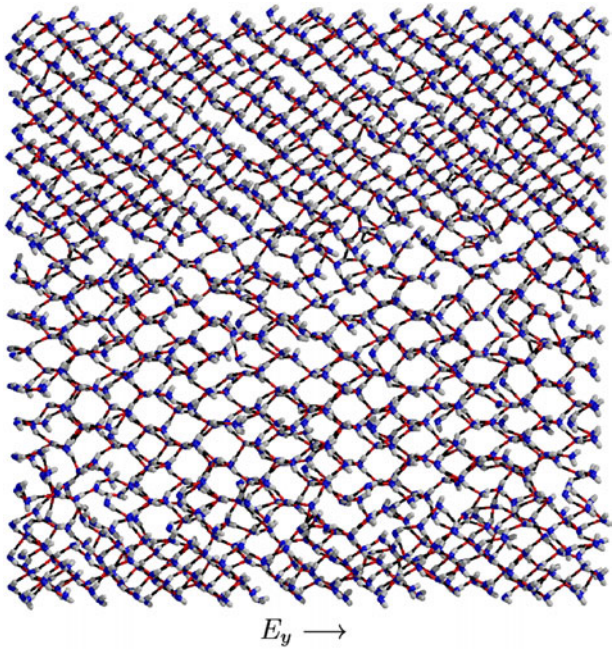

Figure 12. (Colour online) The instantaneous lateral configuration obtained at $T = 280$ K, $H = 0.92$ nm and $A = 40.96$ nm^2, under the action of an electric field along the y-axis ($|E| = 5.0$ V nm^{-1}) showing the coexistence between two different ice structures. Oxygen atoms are depicted in light grey (blue), hydrogen atoms in grey and the lone pair electron sites in dark grey (red).

second maximum, due to the second shell of nearest neighbours, at around $r = 0.37$ nm. In contrast, the curve for $A = 46.24$ nm^2 has a minimum at $r = 0.37$ nm. As mentioned before, this is in agreement with experimental observations from studies of the structure of water in a hydrogel [62, 63], of water in contact with a hydrophobic surface [66] and of the high-density amorphous ice [71]. The strong discontinuity observed is in contrast to the behaviour of a similar transition, between two confined solid phases with different symmetries, found for a hard sphere system [97]. The difference can be attributed to the deep attractive well of the intermolecular interactions between the water molecules that favours a first-order transition.

Additional simulations at other values of plate separations were performed. For some values of H no crystallization was observed. However, for $H = 1.14$, 1.36 and 1.86 nm crystallization due to the application of the electric field was observed. The density of the ice phases obtained is similar to that of the low-density ice phase found at $H = 0.92$ nm. The structure corresponds to proton ordered cubic ice [96]. Freezing of confined water, as observed by x-ray diffraction measurements [98, 99], gives rise to the cubic ice phase instead of the ordinary hexagonal ice.

5. Discussion

We have shown that it is possible to induce the sequential freezing and melting of a monolayer and a bilayer of water by varying the distance between the confining walls. Particles under confinement exhibit large oscillations in density, which in turn correlate with oscillations in the solvation forces, as a function of H, associated with transitions between consecutive layers. Since ordinary ice, I_h, is sensitive to density (e.g. melting can be induced upon increasing the pressure), the alternation of water and ice phases as a function of H in confined

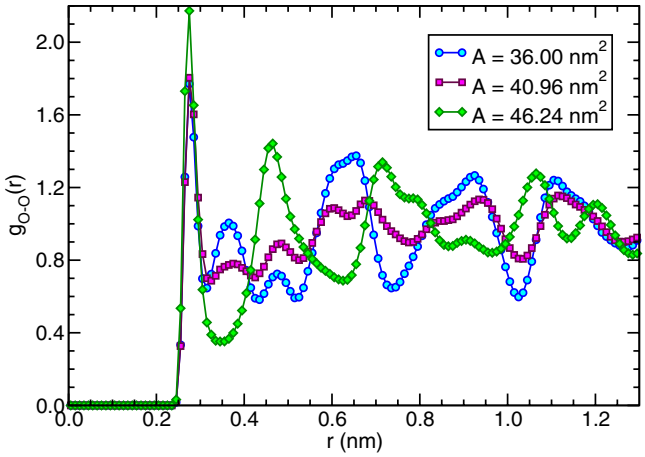

Figure 13. The oxygen–oxygen pair correlation function for the two phases of ice found at $A = 46.24$ (cubic ice) and 36.00 nm^2 (high-density rhombic ice). Also plotted is the pair correlation function for a system of these phases in coexistence, $A = 40.96$ nm^2 (shown in figure 12). The high-density rhombic ice is characterized by a hump at $r = 0.37$ nm.

geometries can be understood in terms of the oscillations in density. However, since the space is inhomogeneous and is divided into lateral and transverse subspaces, the density itself does not serve as a suitable thermodynamic variable. The crystalline phase of water requires the formation of an extensive hydrogen bonding network. The energy of a hydrogen bond is sensitive to variation in the bond length and bond angle [100]. Therefore, the space within which the system is confined needs to allow a suitable geometry for optimal hydrogen bond formation so that the enthalpy gain overcomes the entropy loss of the freezing process. Indeed it is shown that a monolayer of water can only freeze under ambient conditions when it is coupled to a linear buckling transition. By exploiting an ordered out-of-plane displacement of the molecules in the buckled phase the distortion of the hydrogen bonds is minimized. Experimental support for such a phenomenon comes from studies using a mercury/water/mercury tunnel junction at $T = 265$ K where it was found that the Young's modulus of two-dimensional ice shows a maximum value (of ∼20% of bulk ice I_h) with a strong discontinuity as H is increased from 0.50 to 0.80 nm [60]. An optimal distance between the confining walls was also necessary for crystallization to take place in a bilayer and a trilayer of liquid water. In the later case, application of an electric field in the direction parallel to the walls was needed. This shows that the synergistic effects of confinement and electric fields can be used in concert to manipulate the properties of water, which may have possible applications such as in manipulating solutions within high-density microfluidic chips [101].

The transitions that we observed of the freezing and melting of water confined to a slab geometry are first order [37, 61], similar to that observed in the bulk. However, the character of the melting transition in such quasi-two-dimensional systems is proposed to be fundamentally different from that in three dimensions. The different behaviour emerges as a consequence of the loss of long range translational order (in the limit $r \rightarrow \infty$) of a two-dimensional solid [102–106]. According to the Kosterlitz–Thouless–Halperin–Nelson–Young (KTHNY) theory [107–111], two-dimensional solids melt via two sequential continuous phase transitions. It predicts a new phase between the liquid phase and the solid phase, the so-called hexatic phase. The KTHNY theory of melting in two dimensions is not based on any particular choice of intermolecular potential energy function; it remains valid for any system which can be characterized as a deformable elastic medium. However, the transition sequence described is

not the only possible mechanism for two-dimensional melting. For example, it is in principle possible for the KTHNY scenario to be pre-empted by grain boundary induced melting, as has been suggested by Chui [112]. In this case, the melting is predicted to be direct first order. In the confined water systems that we studied, this mechanism is more suitable for describing the melting/freezing process.

There is a fundamental difference between the amorphous structure of the liquid phase and the ordered structure of the crystalline phase. Nevertheless, it has been argued that this difference is only in the degree of order rather than a qualitative difference [113]. Thus, the solid and the liquid states of matter share the same local (short range) structure. A phase transition between two liquid phases in a one-component system is possible if the local order of the two liquid phases is different. Thus, if the system supports two different solid structures (normally two that differ in density) then it is reasonable to expect a liquid–liquid transition. Two crystalline phases of water were observed for a trilayer system under the action of an electric field. The local structure of the two ice phases found is similar to the local structure of the two phases of bilayer of liquid water found in the absence of an external field. The difference between the two liquid phases is in the local ordering at the level of the second shell of nearest neighbours and in the transverse density profile. In both the liquid and solid phases at high densities, the second peak, which gives information about the local arrangement of the oxygen atoms, is shifted toward lower values of interparticle separation ($r \sim 0.37$–0.41 nm). In these phases, larger distortions of hydrogen bond angles are observed. However, the first peak in the radial distribution function is hardly affected by the density increase. This similarity between the local structure of the liquid phase and the short range structure of the solid phase might be stronger in water due to the deep attractive well characteristic of hydrogen bond interactions.

Studies of water confined to a pore of Vycor glass indicate that the nature of the dynamics of the water in the first two layers from the substrate is different to that of bulk liquid water [114, 115]. In particular, it is found that the confined water exhibits similarities in dynamics to that observed in glass forming liquids [116]. A third dynamical relaxation time appears at intermediate times due to the cage effect. In addition, the single-particle displacement distribution deviates from Gaussian form, indicating correlated motions in the system. The origin of this behaviour could be the spatial geometry of the system and/or the interactions of the water molecules with the surface. Very similar behaviour has been observed experimentally in a quasi-two-dimensional colloid suspension [117, 118] and computationally for hard spheres and Lennard-Jones particles [119–122]. However, in the simulations of water confined to a slab geometry with weak water–wall interactions such behaviour was not observed under ambient conditions [37]. Therefore, it seems that fundamental dynamical and thermodynamical properties of water confined only by geometrical constraints can be altered by the presence of surfaces that form hydrogen bond interactions with the water molecules.

References

[1] Hansen J P and McDonald I R 1986 *Theory of Simple Liquids* 2nd edition (London: Academic)
[2] Horn R G and Israelachvili J N 1981 *J. Chem. Phys.* **75** 1400
[3] Christenson H K 1983 *J. Chem. Phys.* **78** 6906
[4] Israelachvili J N, McGuiggan P M and Homola A M 1988 *Science* **240** 189
[5] Demirel A L and Granick S 1996 *Phys. Rev. Lett.* **77** 2261
[6] Antognozzi M, Humphris A D L and Miles M J 2001 *Appl. Phys. Lett.* **78** 300
[7] Henderson D, Abraham F F and Barker J A 1976 *Mol. Phys.* **31** 1291
[8] Fischer J and Methfessel M 1980 *Phys. Rev.* A **22** 2836
[9] Zhou Y and Stell G 1989 *Mol. Phys.* **66** 767
[10] Peterson B K, Gubbins K E, Heffelfinger G S, Marconi U M B and van Swol F 1988 *J. Chem. Phys.* **88** 6487
[11] Kierlik E and Rosinberg M L 1990 *Phys. Rev.* A **42** 3382

[12] Abraham F F 1978 *J. Chem. Phys.* **68** 3713
[13] Snook I K and van Megen W 1980 *J. Chem. Phys.* **72** 2907
[14] Toxvaerd S 1981 *J. Chem. Phys.* **74** 1998
[15] Magda J J, Tirrell M and Davis H T 1985 *J. Chem. Phys.* **83** 1888
[16] Schoen M, Diestler D J and Cushman J H 1987 *J. Chem. Phys.* **87** 5464
[17] Schoen M, Hess S and Diestler D J 1995 *Phys. Rev.* E **52** 2587
[18] Gao J, Luedtke W D and Landman U 1997 *Phys. Rev. Lett.* **79** 705
[19] van Alsten J and Granick S 1988 *Phys. Rev. Lett.* **61** 2570
[20] van Alsten J and Granick S 1990 *Langmuir* **6** 214
[21] Gee M L, McGuiggan P M, Israelachvili J N and Homola A M 1990 *J. Chem. Phys.* **93** 1895
[22] Klein J and Kumacheva E 1995 *Science* **269** 816
[23] Klein J and Kumacheva E 1998 *J. Chem. Phys.* **108** 6996
[24] Hu H-W, Carson G A and Granick S 1991 *Phys. Rev. Lett.* **66** 2758
[25] Rhykerd C L, Schoen M, Diestler D J and Cushman J H 1987 *Nature* **330** 461
[26] Thompson P A, Grest G S and Robbins M O 1992 *Phys. Rev. Lett.* **68** 3448
[27] Hug J E, van Swol F and Zukoski C F 1995 *Langmuir* **11** 111
[28] Cui S T, Cummings P T and Cochran H D 2001 *J. Chem. Phys.* **114** 7189
[29] Ayappa K G and Ghatak C 2002 *J. Chem. Phys.* **117** 5373
[30] Bitsanis I A and Pan C 1993 *J. Chem. Phys.* **99** 5520
[31] Bernal J D and Fowler R H 1933 *J. Chem. Phys.* **1** 515
[32] Kamb B 1973 Crystallography of ice *Physics and Chemistry of Ice* ed E Whalley, S J Jones and L W Gold (Ottawa: Royal Society of Canada) pp 28–41
[33] Hobbs P V 1974 *Ice Physics* (Oxford: Clarendon)
[34] Whalley E 1976 The hydrogen bond in ice *The Hydrogen Bond* ed P Schuster, G Zundel and C Sandorfy (Amsterdam: North-Holland) pp 1427–70
[35] Mahoney M W and Jorgensen W L 2000 *J. Chem. Phys.* **112** 8910
[36] Berendsen H J C, Postma J P M, van Gunsteren W F, DiNola A and Haak J R 1984 *J. Chem. Phys.* **81** 3684
[37] Zangi R and Mark A E 2003 *Phys. Rev. Lett.* **91** 025502
[38] Mahoney M W and Jorgensen W L 2001 *J. Chem. Phys.* **114** 363
[39] Ogawa T 1983 *J. Phys. Soc. Japan* **52** (Suppl.) 167
[40] van Winkle D H and Murray C A 1986 *Phys. Rev.* A **34** 562
[41] Murray C A, Sprenger W, Seshadri R and Cerise J E 1995 Dynamical buckling transitions of confined colloidal monolayer *MRS Symp.: Dynamics in Small Confining Systems* vol 366, ed J M Drake, S M Trolan, J Klafter and R Kopelman (Pittsburgh, PA: Materials Research Society) pp 163–72
[42] Neser S, Palberg T, Bechinger C and Leiderer P 1997 *Prog. Colloid Polym. Sci.* **104** 194
[43] Schmidt M and Löwen H 1997 *Phys. Rev.* E **55** 7228
[44] Zangi R and Rice S A 1998 *Phys. Rev.* E **58** 7529
[45] Neser S, Bechinger C, Leiderer P and Palberg T 1997 *Phys. Rev. Lett.* **79** 2348
[46] Zangi R and Rice S A 2000 *Phys. Rev.* E **61** 660
[47] Pauling L 1935 *J. Am. Chem. Soc.* **57** 2680
[48] Bergman R, Swenson J, Börjesson L and Jacobsson P 2000 *J. Chem. Phys.* **113** 357
[49] Hu J, Xiao X-D, Ogletree D F and Salmeron M 1995 *Science* **268** 267
[50] Hu J, Xiao X-D, Ogletree D F and Salmeron M 1995 *Surf. Sci.* **344** 221
[51] Odelius M, Bernasconi M and Parrinello M 1997 *Phys. Rev. Lett.* **78** 2855
[52] Miranda P B, Xu L, Shen Y R and Salmeron M 1998 *Phys. Rev. Lett.* **81** 5876
[53] Park S-H and Sposito G 2002 *Phys. Rev. Lett.* **89** 085501
[54] Lilach Y, Romm L, Livneh T and Asscher M 2001 *J. Phys. Chem.* B **105** 2736
[55] Feibelman P J 2002 *Science* **295** 99
[56] Marmier A *et al* 1998 *J. Chem. Phys.* **109** 3245
[57] Meyer H, Entel P and Hafner J 2001 *Surf. Sci.* **488** 177
[58] Janiak C and Scharmann T G 2002 *J. Am. Chem. Soc.* **124** 14010
[59] Porter J D and Zinn-Warner A S 1993 *J. Phys. Chem.* **97** 1190
[60] Porter J D and Zinn-Warner A S 1994 *Phys. Rev. Lett.* **73** 2879
[61] Zangi R and Mark A E 2003 *J. Chem. Phys.* **119** 1694
[62] Gorbaty Y E and Demianets Y N 1985 *Mol. Phys.* **55** 571
[63] Bosio L, Johari G P, Oumezzine M and Teixeira J 1992 *Chem. Phys. Lett.* **188** 113
[64] Bruni F, Ricci M A and Soper A K 1998 *J. Chem. Phys.* **109** 1478
[65] Soper A K, Bruni F and Ricci M A 1998 *J. Chem. Phys.* **109** 1486

[66] Bellissent-Funel M-C, Sridi-Dorbez R and Bosio L 1996 *J. Chem. Phys.* **104** 10023
[67] Poole P H, Sciortino F, Essmann U and Stanley H E 1992 *Nature* **360** 324
[68] Stanley H E *et al* 2002 *Physica* A **306** 230
[69] Yamada M, Mossa S, Stanley H E and Sciortino F 2002 *Phys. Rev. Lett.* **88** 195701
[70] Mishima O, Calvert L D and Whalley E 1985 *Nature* **314** 76
[71] Bizidi A, Bosio L, Defrain A and Oumezzine M 1987 *J. Chem. Phys.* **87** 2225
[72] Katayama Y *et al* 2000 *Nature* **403** 170
[73] Meyer M and Stanley H E 1999 *J. Phys. Chem.* B **103** 9728
[74] Brovchenko I, Geiger A and Oleinikova A 2001 *Phys. Chem. Chem. Phys.* **3** 1567
[75] Franzese G, Malescio G, Skibinsky A, Buldyrev S V and Stanley H E 2002 *Phys. Rev.* E **66** 051206
[76] Raviv U, Laurat P and Klein J 2001 *Nature* **413** 51
[77] Kolodziej H A, Jones B P and Davies M 1975 *J. Chem. Soc. Faraday Trans.* II **71** 269
[78] Watts R O 1981 *Chem. Phys.* **57** 185
[79] Alper H E and Levy R M 1990 *J. Phys. Chem.* **94** 8401
[80] Watanabe M, Brodsky A M and Reinhardt W P 1991 *J. Phys. Chem.* **95** 4593
[81] Kornyshev A A and Sutmann G 1997 *Phys. Rev. Lett.* **79** 3435
[82] Yeh I-C and Berkowitz M L 1999 *J. Chem. Phys.* **110** 7935
[83] Gavish M, Wang J-L, Eisenstein M, Lahav M and Leiserowitz L 1992 *Science* **256** 815
[84] Wilen L 1993 *Science* **259** 1469
[85] Svishchev I M and Kusalik P G 1994 *Phys. Rev. Lett.* **73** 975
[86] Svishchev I M and Kusalik P G 1996 *J. Am. Chem. Soc.* **118** 649
[87] Svishchev I M and Kusalik P G 1996 *Phys. Rev.* B **53** R8815
[88] Borzsak I and Cummings P T 1997 *Phys. Rev.* E **56** R6279
[89] Sutmann G 1998 *J. Electroanal. Chem.* **450** 289
[90] Jung D H, Yang J H and Jhon M S 1999 *Chem. Phys.* **244** 331
[91] Xia X and Berkowitz M L 1995 *Phys. Rev. Lett.* **74** 3193
[92] Kiselev M and Heinzinger K 1996 *J. Chem. Phys.* **105** 650
[93] Vegiri A and Shevkunov S V 2001 *J. Chem. Phys.* **115** 4175
[94] Shevkunov S V and Vegiri A 2002 *THEOCHEM* **593** 19
[95] Drost-Hansen W and Singleton J L 1992 *Fundamentals of Medicinal Cell Biology* (Greenwich, CT: JAI Press)
[96] Zangi R and Mark A E 2004 *J. Chem. Phys.* **120** 7123
[97] Zangi R and Rice S A 2000 *Phys. Rev.* E **61** 671
[98] Bellissent-Funel M-C, Lal J and Bosio L 1993 *J. Chem. Phys.* **98** 4246
[99] Morishige K and Kawano K 1999 *J. Chem. Phys.* **110** 4867
[100] Rao C N R 1972 Theory of hydrogen bonding in water *Water: a Comprehensive Treatise* ed F Frankspages (New York: Plenum) pp 93–149
[101] Thorsen T, Maerkl S J and Quake S R 2002 *Science* **298** 580
[102] Mermin N D and Wagner H 1966 *Phys. Rev. Lett.* **17** 1133
[103] Mermin N D 1968 *Phys. Rev.* **176** 250
[104] Peierls R 1979 *Surprises in Theoretical Physics* (Princeton, NJ: Princeton University Press)
[105] Fröhlich J and Pfister C 1981 *Commun. Math. Phys.* **81** 277
[106] Landau L and Lifshitz E 1986 *Statistical Physics* (Oxford: Pergamom)
[107] Kosterlitz J M and Thouless D J 1972 *J. Phys. C: Solid State Phys.* **5** L124
[108] Kosterlitz J M and Thouless D J 1973 *J. Phys. C: Solid State Phys.* **6** 1181
[109] Halperin B I and Nelson D R 1978 *Phys. Rev. Lett.* **41** 121
[110] Nelson D R and Halperin B I 1979 *Phys. Rev.* B **19** 2457
[111] Young A P 1979 *Phys. Rev.* B **19** 1855
[112] Chui S T 1983 *Phys. Rev.* B **28** 178
[113] Frenkel J 1946 *Kinetic Theory of Liquids* (Oxford: Oxford University Press)
[114] Gallo P, Rovere M and Spohr E 2000 *J. Chem. Phys.* **113** 11324
[115] Gallo P, Rovere M and Spohr E 2000 *Phys. Rev. Lett.* **85** 4317
[116] Donati C *et al* 1998 *Phys. Rev. Lett.* **80** 2338
[117] Marcus A H, Schofield J and Rice S A 1999 *Phys. Rev.* E **60** 5727
[118] Cui B, Lin B and Rice S A 2001 *J. Chem. Phys.* **114** 9142
[119] Hurley M M and Harrowell P 1995 *Phys. Rev.* E **52** 1694
[120] Zangi R and Rice S A 2003 *Phys. Rev.* E **68** 061508
[121] Reichhardt C and Reichhardt C J O 2003 *Phys. Rev. Lett.* **90** 095504
[122] Zangi R and Rice S A 2004 *Phys. Rev. Lett.* **92** 035502